Am J Cancer Res 2026;16(11):4833-4850
www.ajcr.us /ISSN:2156-6976/ajcr0173956

Original Article

LncRNA PCED1B-AS1 promotes cell proliferation and glycolysis in esophageal squamous cell carcinoma by positively regulating KPNA2 via interaction with miR-26a-5p

Lian Gao*, Xiaoming Huang*, Chun Bai*, Jing Lin, Hongbin Wang, Linyan Zhu

*Department of Gastroenterology, Huangshi Central Hospital (Affiliated Hospital of Hubei Polytechnic University), No. 141 Tianjin Road, Huangshi 435000, Hubei, China. *Equal contributors.*

Received May 11, 2026; Accepted October 25, 2026; Epub November 15, 2026; Published November 30, 2026

Abstract: PC-esterase domain containing 1B antisense RNA 1 (PCED1B-AS1), a glycolysis-associated long non-coding RNA (lncRNA), has been implicated in tumor metabolism. However, its functional role and underlying mechanism in esophageal squamous cell carcinoma (ESCC) remain largely unexplored. The expression levels of PCED1B-AS1, miR-26a-5p, and karyopherin subunit alpha 2 (KPNA2) were quantified by reverse transcription quantitative polymerase chain reaction (RT-qPCR), and KPNA2 protein expression was analyzed using Western blotting. Cell viability and proliferative capacity were assessed using cell counting kit-8 (CCK-8) and colony formation assays, and apoptosis was measured by flow cytometry. The binding of miR-26a-5p to KPNA2 or PCED1B-AS1 was validated by dual-luciferase reporter assays. RIP assays confirmed the molecular interactions among PCED1B-AS1, miR-26a-5p, and KPNA2. Glucose uptake and lactate production were measured using commercial kits. Extracellular acidification rate (ECAR) and oxygen consumption rate (OCR) were quantified via Seahorse XFe96 extracellular flux analysis. A xenograft mouse model was established to explore the *in vivo* role of PCED1B-AS1. The results showed that PCED1B-AS1 was markedly upregulated in ESCC cell lines. Knockdown of PCED1B-AS1 strongly suppressed cell proliferation and promoted apoptosis. Functionally, silencing PCED1B-AS1 attenuated glycolysis, as evidenced by reduced glucose uptake, lactate production, and ECAR, while enhancing oxidative phosphorylation. PCED1B-AS1 acted as a miR-26a-5p sponge, leading to upregulation of its direct target KPNA2. The suppressive effects of PCED1B-AS1 knockdown on ESCC cell growth and glycolysis were reversed by miR-26a-5p inhibitor or KPNA2 overexpression. In contrast, the oncogenic effects of PCED1B-AS1 on ESCC cell malignancy were counteracted by KPNA2 knockdown. Moreover, silencing PCED1B-AS1 effectively inhibited xenograft growth in ESCC. In summary, PCED1B-AS1 promotes ESCC progression and glycolysis by acting as a competing endogenous (ceRNA) that sponges miR-26a-5p, thereby upregulating KPNA2 expression.

Keywords: PC-esterase domain containing 1B antisense RNA 1, miR-26a-5p, karyopherin subunit alpha 2, esophageal squamous cell carcinoma, glycolysis

Introduction

Esophageal cancer poses a significant global health challenge, ranking ninth in incidence and sixth in mortality among all cancers. Histologically, esophageal squamous cell carcinoma (ESCC) is the predominant subtype [1-3], accounting for nearly 90% of all cases worldwide, with more than half of these cases occurring in China. It is an exceptionally aggressive malignancy characterized by rapid progression, a high propensity for lymph node metastasis, and a tumor location typically in the upper to middle esophagus [4, 5]. Because early specific symptoms such as dysphagia are often absent, patients are frequently diagnosed at advanced stages, leading to a notoriously poor prognosis with low 5-year survival rates. The pathogenesis of ESCC is closely linked to chronic mucosal exposure to carcinogens, including tobacco smoke, alcohol, betel nut, and caustic chemical injury, which collectively drive sustained inflammation and cellular damage [6, 7]. Although current standard therapies for locally advanced

https://doi.org/10.62347/KCZZ3637

disease, such as radiotherapy and definitive chemoradiotherapy, are employed, their efficacy remains limited, and treatment resistance is common [8-11]. Unraveling the molecular underpinnings of ESCC and discovering actionable therapeutic targets remain critical priorities for improving patient prognosis.

Long non-coding RNAs (lncRNAs) have emerged as pivotal regulators of gene expression and cellular function in cancer biology. In ESCC, evidence underscores their critical roles in tumor initiation, progression, and therapeutic response [12-14]. Clinically, specific lncRNAs are significantly correlated with key clinicopathological features such as tumor stage [15], differentiation status [16], metastasis [17], and patient survival outcomes [18]. Functionally, they orchestrate diverse malignant phenotypes in ESCC cells, including uncontrolled proliferation [19], evasion of apoptosis [20], and glycolysis [21]. Notably, dysregulated lncRNAs are increasingly implicated in modulating glycolytic metabolism, a hallmark of cancer, in the ESCC context [14]. This metabolic reprogramming enables cancer cells to favor glycolysis even under aerobic conditions, thereby rapidly generating energy and biosynthetic precursors to support uncontrolled proliferation [22-24]. Importantly, such enhanced glycolytic flux is closely associated with increased resistance to chemo- and radiotherapy, further underscoring its critical role in tumor progression and therapeutic failure. Among these, lncRNA PC-esterase domain containing 1B antisense RNA 1 (PCED1B-AS1) has recently been identified as a glycolysis-associated molecule that promotes tumor progression in glioblastoma [25]. Bioinfor-matic analyses further reveal a significant upregulation of PCED1B-AS1 in esophageal carcinoma (ESCA) tissues. Nevertheless, its precise biological function, molecular mechanism, and relevance to glycolysis in ESCC remain completely unexplored.

LncRNAs frequently exert their biological effects through a competing endogenous RNA (ceRNA) mechanism, acting as molecular sponges that sequester miRNAs and consequently upregulate the expression of their target genes [26-28]. Emerging evidence has demonstrated that this ceRNA axis plays a critical role in the pathogenesis and malignant progression of multiple tumor types. To elucidate the molecular mechanism of PCED1B-AS1 in ESCC, we first used the LncBase v3 database and identified the top five candidate miRNAs potentially interacting with PCED1B-AS1. Among these, miR-26a-5p was selected for further investigation because of its documented tumor-suppressive role in ESCC [29, 30]. Subsequently, bioinformatic prediction revealed karyopherin subunit alpha 2 (KPNA2) as one of the top potential targets of miR-26a-5p. KPNA2 has been documented to be overexpressed across diverse cancer types, where it drives both tumor progression and glycolytic metabolism. For instance, in lung adenocarcinoma, KPNA2 facilitates glycolysis by promoting cellular myelocytomatosis oncogene (MYC) nuclear translocation [31]. Notably, in ESCC, KPNA2 has been shown to be upregulated by another lncRNA, small nucleolar RNA host gene 8 (SNHG8), through sponging of miR-411 [32]. However, whether PCED1B-AS1 can regulate KPNA2 via miR-26a-5p, and whether this axis contributes to glycolytic metabolism and malignant progression in ESCC, remains entirely unknown.

The study aims to determine how PCED1B-AS1 contributes to ESCC progression by regulating cell proliferation and glycolysis, and to clarify the molecular basis of these effects. Our findings may expand the current understanding of ESCC pathogenesis and identify PCED1B-AS1 as a potential therapeutic target in this malignancy.

Materials and methods

Bioinformatics analysis

Gene expression profiling interactive analysis (GEPIA; http://gepia.cancer-pku.cn/) was used to evaluate the expression of PCED1B-AS1 in ESCA. DNA intelligent analysis (DIANA)-LncRNA Base (LncBase) v3 (https://diana.e-ce.uth.gr/lncbasev3) was used to predict the downstream miRNAs of PCED1B-AS1. Encyclopedia of RNA interactomes (ENCORI; https://rnasysu.com/encori/) was used to examine the expression of miR-26a-5p and KPNA2 and to predict the target genes of miR-26a-5p in ESCA tissues. Additionally, the expression correlation between miR-26a-5p and KPNA2 in ESCA samples was analyzed using ENCORI. All analyses were performed using the standard workflows provided by the respective platforms.

Cell culture

All cells were cultured in Roswell Park Memorial Institute (RPMI)-1640 medium (IMC-202, IMMOCELL, Xiamen, China) supplemented with 10% FBS and 1% penicillin/streptomycin at 37°C in a humidified 5% CO_2 incubator. The following cell lines were used: normal human esophageal epithelial cells (HEEC, FY-22FN-2313) from FUYUBIO (Shanghai, China), and ESCC cell lines KYSE150 (SNL-344), TE-1 (SNL-209), and Eca109 (SNL-511) from SUNNCELL (Wuhan, China). All cell lines were authenticated by short tandem repeat (STR) profiling, and periodic mycoplasma detection was routinely conducted during cell passaging. All mycoplasma test results were negative throughout the experiments. Cells within low passage numbers (passage 3-10) were used for all functional assays.

Cell transfection

GeneChem (Shanghai, China) constructed gene-specific short hairpin RNAs (shRNAs) targeting PCED1B-AS1 (sh-PCED1B-AS1#1 and sh-PCED1B-AS1#2) and the corresponding negative control (sh-NC); pcDNA3.1 vectors containing the full-length sequence of PCED1B-AS1 or KPNA2 (OE-PCED1B-AS1 or OE-KPNA2) and empty pcDNA3.1 vector as control; an shRNA targeting KPNA2 (sh-KPNA2) paired with its negative control (sh-NC), as well as miR-26a-5p mimics, miR-26a-5p inhibitor, and their respective negative controls (NC mimics and NC inhibitor). Transfection was performed using Lipofectamine 3000 reagent (G0Y-C3099, Goybio, Shanghai), and each plasmid construct or oligonucleotide transfected individually.

RNA fractionation assay

Nuclear and cytoplasmic fractions were obtained using the Nuclear/Cytosol Fractionation Kit (ab289882, Abcam, UK), according to the manufacturer's instructions. RNA was extracted from the separated nuclear and cytoplasmic fractions, and the subcellular distribution of PCED1B-AS1, cytoplasmic reference Glyceraldehyde-3-phosphate dehydrogenase (GAPDH), and nuclear reference U6 was quantified by reverse transcript quantitative polymerase chain reaction (RT-qPCR) to calculate the relative percentage of each transcript in the cytoplasmic and nuclear compartments.

RT-qPCR

Total RNA was extracted using TRIzol reagent (AAB0029A, Seebio, Shanghai). RNA concentration and purity were determined with a NanoDrop 2000c spectrophotometer (Thermo Fisher, Carlsbad, CA, USA). A total of 2 μg of qualified total RNA was reverse-transcribed into complementary DNA (cDNA) using the RevertAid First Strand cDNA Synthesis Kit (Thermo Fisher). The qPCR was performed on an ABI 7500 Fast Real-Time PCR System (Applied Biosystems) with SYBR Green PCR Master Mix (Takara, Japan). GAPDH was used as the internal reference for mRNA and lncRNA, whereas U6 snRNA served as the reference for miRNA. All primers were designed and synthesized by RiboBio (Guangzhou, China), and their sequences are listed in Table S1.

Cell counting kit-8 (CCK-8) assay

After transfection, cells were seeded into 96-well plates and cultured for 24, 48, or 72 h. At each predetermined time point, 10 μL of CCK-8 solution (CK001, LABLEAD, Beijing, China) was added to each well. Plates were incubated at 37°C for 4 h, and the absorbance value at 450 nm was measured using a Tecan Infinite M1000 Pro microplate reader (Männedorf, Switzerland).

Colony formation assay

KYSE150 and Eca109 cells were seeded into six-well plates and maintained for approximately 2 weeks to allow colony formation. Afterwards, cells were fixed with 4% paraformaldehyde (60536ES, Shanghai) for 15 min, stained with 0.1% crystal violet, and rinsed gently with phosphate-buffered saline (PBS). Visible colonies were imaged and counted using ImageJ software.

Cell apoptosis assay

Cell apoptosis was detected using the Annexin V-fluorescein isothiocyanate/propidium iodide (Annexin V-FITC/PI) Apoptosis Detection Kit (A211-01, Vazyme, Nanjing, China) following the manufacturer's protocol. Briefly, KYSE150 and Eca109 cells were seeded into six-well plates (2×10^5 cells/well) and cultured for the indicated time periods. Cells were harvested, washed twice with pre-cooled PBS, and resus-

pended in 100 μL of 1× binding buffer. Cells were then stained with 5 μL of Annexin V-FITC and 5 μL of PI for 15 min at room temperature under dark conditions. An additional 400 μL of 1× binding buffer was added before flow cytometry analysis. Samples were acquired on a BD FACSCalibur flow cytometer (Franklin Lakes, NJ, USA), and data were analyzed using FlowJo software.

Measurement of glucose uptake and lactate production levels

Glycolytic capacity was assessed by detecting glucose uptake and lactate secretion using commercial assay kits. Glucose consumption in the culture supernatant were quantified with a colorimetric Glucose Uptake Assay Kit (ab136955, Abcam, Shanghai). L-lactate concentrations were measured using the L-Lactate Assay Kit (ab65330, Abcam). All experimental operations were performed strictly in accordance with the manufacturer's protocols. Optical signals were recorded at Ex/Em=570/610 nm using a TECAN SPARK microplate reader.

Extracellular acidification rate (ECAR) and oxygen consumption rate (OCR) detection

A Seahorse XFe96 extracellular flux analyzer (Seahorse Bioscience, USA) was applied to measure ECAR and OCR. Briefly, cells were harvested, counted, and seeded into Seahorse XF96 cell culture microplates (1×10^4 cells/well). After 10-h of incubation to allow cell attachment, the Seahorse XF Glycolysis Stress Test Kit and the Seahorse XF Cell Mito Stress Test Kit (Agilent, USA) were used to determine ECAR and OCR, respectively. For ECAR detection, glucose, oligomycin, and 2-DG were sequentially injected at designated time points. For OCR measurement, oligomycin, FCCP, and a mixture of antimycin A plus rotenone were sequentially added following the manufacturer's protocol.

RNA immunoprecipitation (RIP) assay

The RIP assay was carried out using the Magna RIP Kit (Millipore, MA, USA) as instructed by the manufacturer. Cells were lysed in the lysis buffer. The lysates were incubated overnight at 4°C with Pierce™ Protein A/G Magnetic Beads (Thermo Fisher) pre-bound with anti-Ago2 antibody (ab32381, Abcam) or normal rabbit IgG (ab188776, Abcam) serving as the negative control. The magnetic beads were captured with a magnetic stand and thoroughly washed with the lysis buffer. Co-precipitated RNAs were extracted using TRIzol reagent. The enrichment of target RNAs (PCED1B-AS1, miR-26a-5p, and KPNA2) were quantified by RT-qPCR. Relative RNA enrichment was calculated using the $2^{-\Delta\Delta Ct}$ method, with input RNA samples set as the normalization control.

Luciferase reporter assay

For dual-luciferase reporter assays, wild-type (WT) and mutant (MUT) fragments of PCED1B-AS1 or the KPNA2 3'-untranslated region (3'UTR) containing the predicted miR-26a-5p binding sites were cloned into the pGL3 luciferase reporter vector (Promega). The resulting constructs were designated PCED1B-AS1-WT, PCED1B-AS1-MUT, KPNA2-WT, and KPNA2-MUT. These reporter plasmids were co-transfected into ESCC cells together with miR-26a-5p mimics or NC mimics. At 48 h post-transfection, the Dual-Luciferase Reporter Assay System (Promega, WI, USA) was used to measure luciferase activity.

Western blot analysis

Cells were lysed in radioimmunoprecipitation assay (RIPA) buffer (E-EL-SR002, Elabscience, Wuhan) containing phenylmethylsulfonyl fluoride protease inhibitor. Equal amounts of total protein (20 μg per lane) were separated by 10% sodium dodecyl sulfate-polyacrylamide gel electrophoresis. Subsequently, proteins were electrotransferred onto polyvinylidene fluoride membranes under a constant current of 300 mA for 90 min at 4°C. After membrane transfer, non-specific binding sites were blocked with 5% non-fat milk in Tris-buffered saline with Tween 20 for 1 h at room temperature. Membranes were then incubated overnight at 4°C with primary antibodies against KPNA2 (#14372) and GAPDH (#2118) (Cell Signaling Technology), both diluted at 1:1000. GAPDH was used as the internal loading control. Next, membranes were incubated with horseradish peroxidase-conjugated anti-rabbit secondary antibody (#7074, dilution: 1:1,000) for 1 h at room temperature. Protein bands were visualized using an enhanced chemiluminescence kit (E-IR-R308, Elabscience, Wuhan). Band intensities were quantified with ImageJ software.

Xenograft assay

A total of 14 female BALB/c nude mice, aged 4-6 weeks, were obtained from Vital River Animal Technology (Beijing, China). The animals were divided into two experimental groups (sh-NC and sh-PCED1B-AS1#1), with seven mice per group. Stably transfected cells were harvested by digestion with 0.25% trypsin, subjected to centrifugation at 2000 rpm for 10 min, and then resuspended in 100 μL of RPMI medium containing approximately 3×10^6 cells. This cell suspension was then injected subcutaneously into the nude mice. Tumor development was observed daily, while tumor dimensions and mouse body weights were recorded every three days. After six weeks, the mice were euthanized via intraperitoneal overdose of sodium pentobarbital (150 mg/kg body weight). Death was confirmed by cervical dislocation following loss of pedal reflex and cessation of respiration. This euthanasia protocol follows the AVMA Guidelines for the Euthanasia of Animals and GB/T 39760-2021, and all animal procedures were performed in strict compliance with our institutional approved animal ethics protocol. Tumor tissues were then collected for preservation. The excised tumor tissues were stored for RT-qPCR, western blotting, and detection of lactic acid content. Animal experiments received approval from the Ethics Committee of Wuhan Myhalic Biotechnology Co., Ltd. (Hubei, China; approval number: HLK-202411295, approval date: November 20, 2024; Supplementary file), and were conducted in accordance with the National Research Council's Guide for the Care and Use of Laboratory Animals.

Statistical analysis

All *in vitro* experiments were repeated in triplicate and independently repeated three times. All quantitative data are presented as mean ± standard deviation (SD). Statistical analyses were conducted using GraphPad Prism. For comparisons involving a single independent factor, one-way analysis of variance (ANOVA) followed by Tukey's *post-hoc* test was applied. For comparisons involving two independent factors, a repeated-measures two-way ANOVA coupled with Sidak's post-hoc test. Notably, repeated-measures ANOVA was utilized for multi-group comparisons involving time as a repeated measurement variable to account for within-subject temporal correlation. A p-value <0.05 was considered statistically significant.

Results

Knockdown of PCED1B-AS1 inhibits ESCC cell viability and proliferation while promoting apoptosis

Bioinformatic analysis using the GEPIA database revealed a marked upregulation of PCED1B-AS1 in ESCC specimens compared with their non-cancerous counterparts (**Figure 1A**). Consistent with these finding, RT-qPCR showed that PCED1B-AS1 expression was drastically elevated in ESCC cell lines relative to the HEEC cell line (**Figure 1B**). To further explore the functional effects of PCED1B-AS1 on ESCC cellular phenotypes, sh-PCED1B-AS1#1 and sh-PCED1B-AS1#2 plasmids were constructed and transfected into ESCC cells. RT-qPCR analysis demonstrated that both shRNA constructs effectively silenced PCED1B-AS1 expression, leading to a striking reduction in its relative expression level compared with the negative control sh-NC group in both cell lines (**Figure 1C**). Following verification of successful knockdown, CCK-8 assays revealed that downregulation of PCED1B-AS1 observably suppressed the proliferative activity of KYSE150 and Eca109 cells in a time-dependent manner, as evidenced by notably lower optical density values at 24, 48, and 72 h in the sh-PCED1B-AS1 groups than in the sh-NC group (**Figure 1D**). Consistently, colony formation assays further validated that knockdown of PCED1B-AS1 markedly impaired the long-term clonogenic survival ability of ESCC cells, with colonies formed by KYSE150 and Eca109 cells being significantly diminished in the knockdown groups (**Figure 1E**, **1F**). Finally, flow cytometric analysis confirmed that silencing PCED1B-AS1 led to a pronounced elevation in apoptotic cell populations in KYSE150 and Eca109 cells (**Figure 1G**, **1H**).

Silencing of PCED1B-AS1 suppresses ESCC glycolysis

To gain further insight into the role of PCED1B-AS1 in ESCC glycolytic metabolism, we ectopically overexpressed PCED1B-AS1 in TE-1 cells. RT-qPCR analysis verified that transfection of OE-PCED1B-AS1 significantly upregulated PCED1B-AS1 levels, confirming the successful

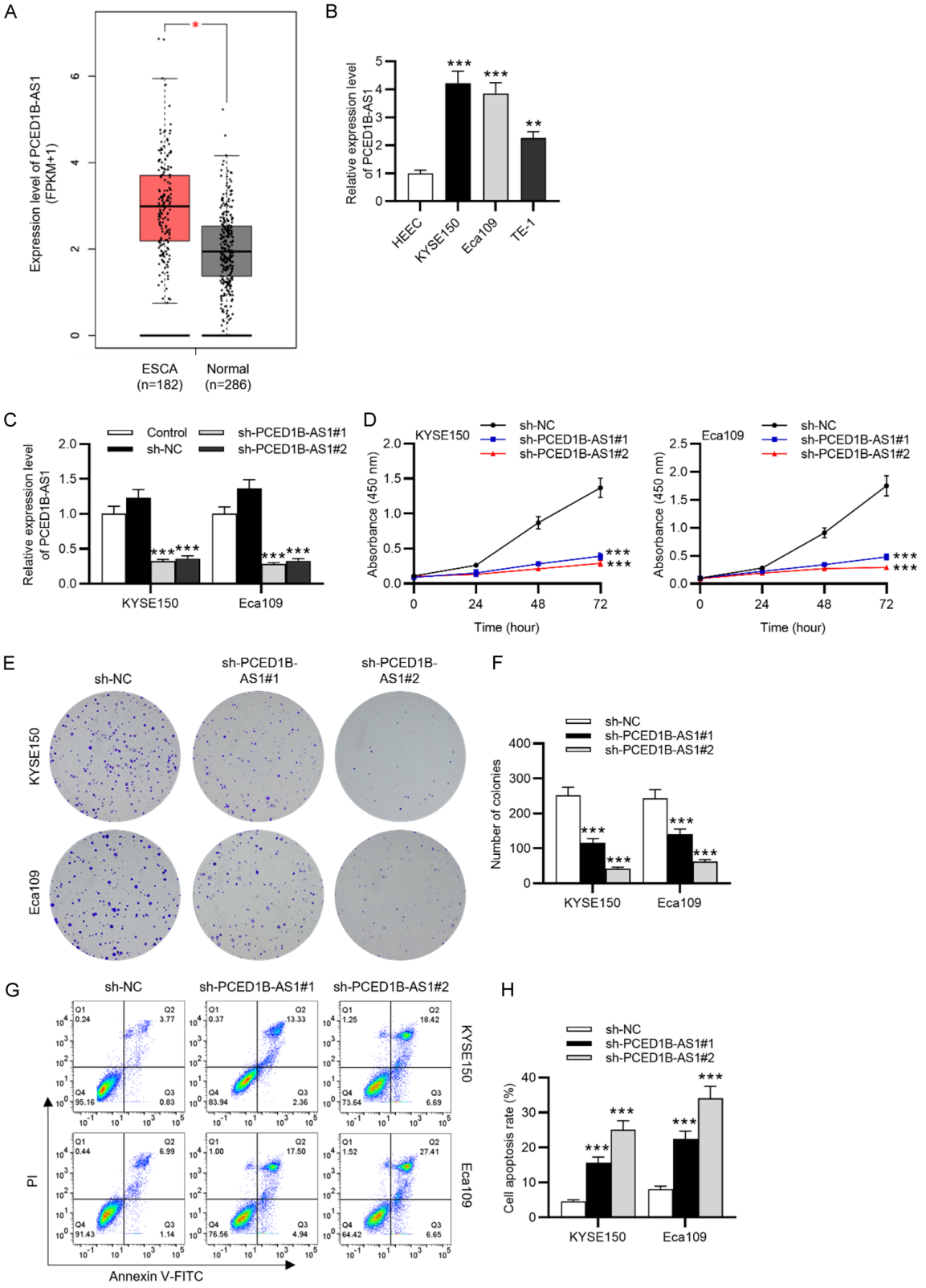


Figure 1. Knockdown of PC-esterase domain containing 1B antisense RNA 1 (PCED1B-AS1) inhibits esophageal squamous cell carcinoma (ESCC) cell viability and proliferation while promoting apoptosis. A. Gene expression profiling interactive analysis (GEPIA) was used to predict PCED1B-AS1 expression in ESCC tissues. B. Reverse transcription quantitative polymerase chain reaction (RT-qPCR) was used to measure PCED1B-AS1 levels in HEEC, KYSE150,

Eca109, and TE-1 cells. C. RT-qPCR was used to detect PCED1B-AS1 levels in KYSE150 and Eca109 cells transfected with short hairpin RNA-negative control (sh-NC), sh-PCED1B-AS1#1, and sh-PCED1B-AS1#2. D. Cell counting kit-8 (CCK-8) assays were used to detect the viability of KYSE150 and Eca109 cells. E, F. Colony formation assays were conducted to assess the proliferation of KYSE150 and Eca109 cells. G, H. Flow cytometry analysis was used to detect the apoptosis of KYSE150 and Eca109 cells. n=3. $^{**}P<0.01$, $^{***}P<0.001$ versus HEEC group or sh-NC group.

construction of the overexpression system (**Figure 2A**). Subsequently, glucose uptake detection showed that overexpression of PCED1B-AS1 markedly enhanced the glucose absorption capacity of TE-1 cells, manifesting as a prominent increase in relative glucose uptake (**Figure 2B**). In contrast, silencing PCED1B-AS1 in KYSE150 and Eca109 cells observably restrained glucose uptake, leading to a striking reduction in intracellular glucose accumulation compared with the sh-NC group (**Figure 2C**). As for lactate production, the end product of glycolysis, overexpression of PCED1B-AS1 significantly boosted lactate secretion in TE-1 cells (**Figure 2D**), whereas knockdown of PCED1B-AS1 dramatically decreased lactate production in both KYSE150 and Eca109 cells (**Figure 2E**). Furthermore, ECAR analysis illustrated that silencing PCED1B-AS1 evidently suppressed both the basal glycolysis level and glycolytic capacity of ESCC cells, leading to a pronounced decline in ECAR values throughout the detection period (**Figure 2F**). In addition, OCR detection revealed that downregulation of PCED1B-AS1 significantly elevated both basal OCR and maximal OCR in KYSE150 cells, indicating a marked enhancement of mitochondrial oxidative respiration and a shift in cellular energy metabolism (**Figure 2G**).

PCED1B-AS1 interacts with miR-26a-5p in ESCC cells

To elucidate whether PCED1B-AS1 exerts its oncogenic effects in ESCC via a ceRNA mechanism, we performed RNA fractionation assays to determine PCED1B-AS1 expression in the cytoplasm and nucleus of ESCC cells. Results of **Figure 3A** reveal that PCED1B-AS1 is primarily located in the cytoplasm of KYSE150 and Eca109 cells. Subsequently, we predicted its downstream miRNAs using the LncBase v3 database and validated the top five candidates by RT-qPCR after PCED1B-AS1 knockdown. Notably, miR-26a-5p expression showed the most dramatic increase in both KYSE150 and Eca109 cells (**Figure 3B**), implying a potential inhibitory interaction between PCED1B-AS1 and miR-26a-5p. We next assessed the endogenous levels of miR-26a-5p in normal HEEC cells and a panel of ESCC cell lines. Compared with HEEC cells, miR-26a-5p expression was substantially reduced in ESCC cells (**Figure 3C**). To further verify the functional interaction, we transfected miR-26a-5p mimics into KYSE150 and Eca109 cells to establish an overexpression model, and RT-qPCR results confirmed that miR-26a-5p expression was strikingly elevated in the mimic group relative to the NC mimic group, validating the successful construction of the overexpression system (**Figure 3D**). Bioinformatic analysis further identified the complementary binding sequences between wild-type PCED1B-AS1 and miR-26a-5p, alongside the designed mutant binding sites of PCED1B-AS1 (**Figure 3E**). The direct interaction between PCED1B-AS1 and miR-26a-5p was validated by dual-luciferase reporter assays: co-transfection with miR-26a-5p mimics markedly suppressed the luciferase activity of the wild-type PCED1B-AS1 reporter, whereas the mutant construct remained unresponsive (**Figure 3F**). Additionally, ENCORI database analysis demonstrated that miR-26a-5p expression was significantly lower in ESCC tissues than in normal counterparts, underscoring the clinical significance of the PCED1B-AS1/miR-26a-5p axis in ESCC (**Figure 3G**).

KPNA2 is a direct target gene of miR-26a-5p in ESCC cells

To identify downstream targets of miR-26a-5p in ESCC, we used the ENCORI database to predict its top five candidate genes. Following miR-26a-5p overexpression in KYSE150 and Eca109 cells, RT-qPCR analysis revealed that only KPNA2 mRNA was significantly downregulated, whereas the other four candidates remained unchanged, identifying KPNA2 as a potential functional target of miR-26a-5p (**Figure 4A**). Subsequently, western blotting analysis further validated that ectopic overexpression of miR-26a-5p observably reduced the protein expression of KPNA2 in both KYSE150 and Eca109 cell lines (**Figure 4B**). Bioinformatic analysis was then applied to predict the complementary binding sequences between miR-26a-5p and the 3'UTR of wild-type KPNA2, and the corresponding mutant binding sites of

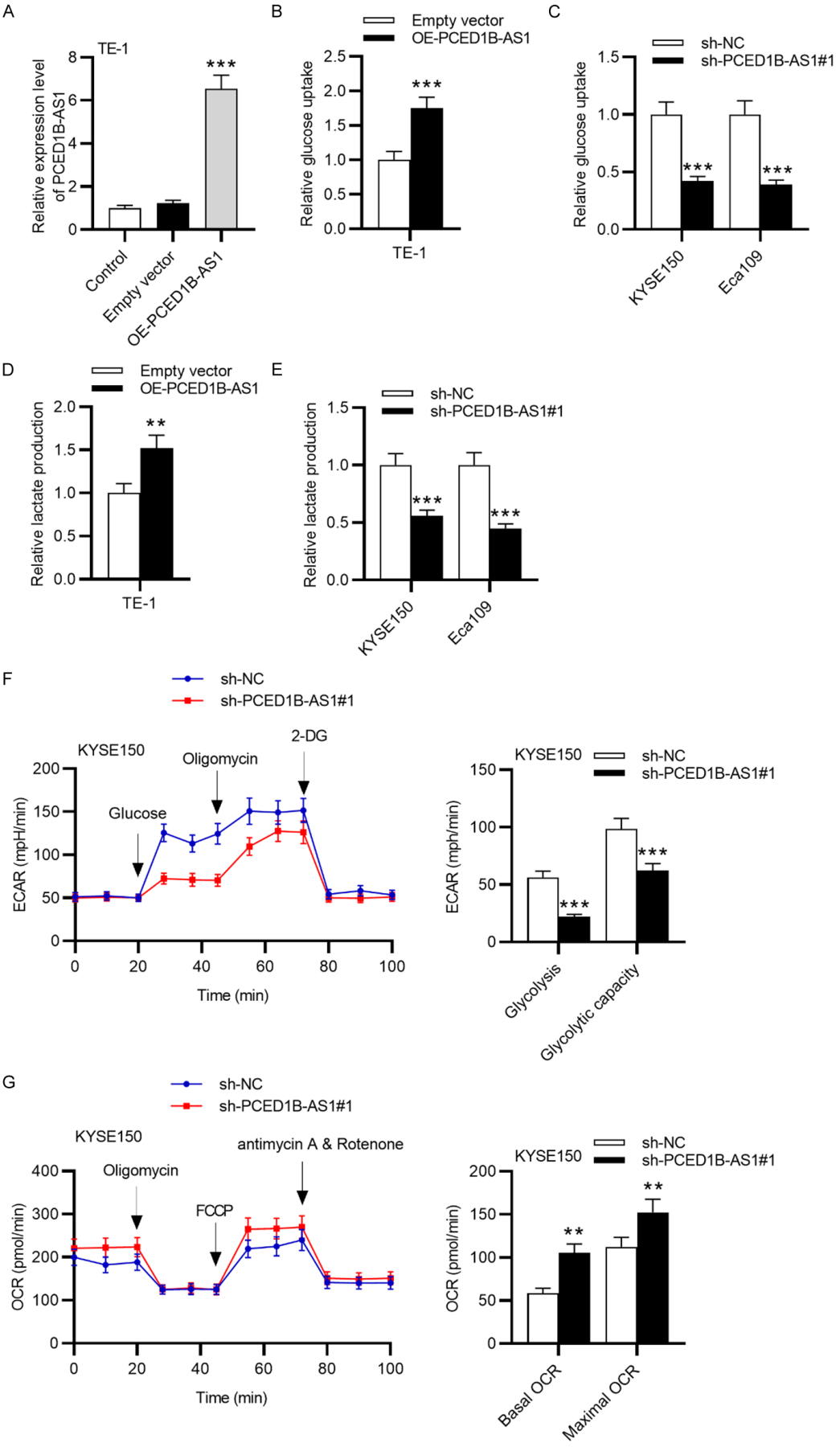

A
TE-1
Relative expression level of PCED1B-AS1
***
Control
Empty vector
OE-PCED1B-AS1
B
Empty vector
OE-PCED1B-AS1
Relative glucose uptake
***
TE-1
C
sh-NC
sh-PCED1B-AS1#1
Relative glucose uptake
***
***
KYSE150
Eca109
D
Empty vector
OE-PCED1B-AS1
Relative lactate production
**
TE-1
E
sh-NC
sh-PCED1B-AS1#1
Relative lactate production
***
***
KYSE150
Eca109
F
sh-NC
sh-PCED1B-AS1#1
KYSE150
Oligomycin
2-DG
Glucose
ECAR (mpH/min)
Time (min)
KYSE150
sh-NC
sh-PCED1B-AS1#1
ECAR (mph/min)
***
***
Glycolysis
Glycolytic capacity
G
sh-NC
sh-PCED1B-AS1#1
KYSE150
Oligomycin
FCCP
antimycin A & Rotenone
OCR (pmol/min)
Time (min)
KYSE150
sh-NC
sh-PCED1B-AS1#1
OCR (pmol/min)
**
**
Basal OCR
Maximal OCR

Figure 2. Silencing of PCED1B-AS1 suppresses ESCC glycolysis. A. RT-qPCR was used to detect PCED1B-AS1 expression in TE-1 cells transfected with empty vector or PCED1B-AS1 overexpression plasmids (OE-PCED1B-AS1). B. Commercial reagent kits were used to measure glucose uptake in TE-1 cells transfected with empty vector and OE-PCED1B-AS1. C. Commercial reagent kits were used to assess glucose uptake in KYSE150 and Eca109 cells transfected with sh-NC or sh-PCED1B-AS1#1. D. Commercial reagent kits were used to detect lactate production in TE-1 cells transfected with empty vector or OE-PCED1B-AS1. E. Commercial reagent kits were used to assess lactate production in KYSE150 and Eca109 cells transfected with sh-NC or sh-PCED1B-AS1#1. F, G. Extracellular acidification rate (ECAR) and oxygen consumption rate (OCR) in KYSE150 cells transfected with sh-NC or sh-PCED1B-AS1#1 were determined using a Seahorse XFe96 extracellular flux analyzer. n=3. $^{**}P<0.01$, $^{***}P<0.001$ versus empty vector or sh-NC group.

KPNA2 were designed accordingly (**Figure 4C**). Dual-luciferase reporter assays demonstrated that miR-26a-5p directly binds to KPNA2, as evidenced by the significant reduction in luciferase activity observed only in cells co-transfected with miR-26a-5p mimics and wild-type KPNA2 reporter, but not in those harboring the mutant construct (**Figure 4D**). Furthermore, RIP assays illustrated that PCED1B-AS1, miR-26a-5p and KPNA2 were all markedly enriched in the Anti-Ago2 antibody group compared with the Anti-IgG control group in both ESCC cell lines, confirming that these three molecules form a functional RNA-induced silencing complex and participate in the ceRNA regulatory network in ESCC (**Figure 4E**). ENCORI database demonstrated that KPNA2 expression was dramatically upregulated in ESCC tissues, suggesting the clinical significance of KPNA2 in ESCC malignant progression (**Figure 4F**). Additionally, ENCORI database analysis revealed that miR-26a-5p and KPNA2 were negatively correlated in ESCC tissues (**Figure 4G**). Consistent with the tissue expression profile, KPNA2 was markedly upregulated at both the transcriptional and translational levels in ESCC cell lines relative to HEEC cells, as depicted in **Figure 4H**. Finally, silencing PCED1B-AS1 in KYSE150 and Eca109 cells resulted in a marked decrease in both KPNA2 mRNA and protein levels, indicating that PCED1B-AS1 positively modulates KPNA2 expression through miR-26a-5p sequestration in ESCC cells (**Figure 4I**).

PCED1B-AS1 promotes ESCC cell proliferation and glycolysis by targeting miR-26a-5p and KPNA2

To verify the regulatory mechanism by which PCED1B-AS1 facilitates ESCC progression through modulation of the miR-26a-5p/KPNA2 axis, rescue experiments were carried out. RT-qPCR and Western blotting assays revealed that knockdown of PCED1B-AS1 markedly diminished the mRNA and protein expression levels of KPNA2, while co-transfection with miR-26a-5p inhibitor or KPNA2 overexpression plasmid markedly reversed this inhibitory effect, restoring KPNA2 expression to a level comparable to the control group (**Figure 5A**). Next, as revealed by CCK-8 assays, PCED1B-AS1 knockdown remarkably inhibited the viability of ESCC cells, whereas inhibition of miR-26a-5p or enforced overexpression of KPNA2 effectively abrogated the proliferation-restraining effect induced by PCED1B-AS1 knockdown, leading to a notable recovery in cellular growth activity (**Figure 5B**). In terms of glycolytic metabolism, glucose uptake detection showed that PCED1B-AS1 depletion observably reduced the glucose absorption ability of KYSE150 cells, and this reduction was significantly overturned by miR-26a-5p inhibition or KPNA2 overexpression (**Figure 5C**). Consistently, lactate production, the key end product of glycolysis, was decreased following PCED1B-AS1 knockdown, and the suppressive effect was markedly rescued by blocking miR-26a-5p or upregulating KPNA2 (**Figure 5D**). Furthermore, ECAR analysis illustrated that knockdown of PCED1B-AS1 distinctly attenuated both the basal glycolysis level and glycolytic capacity of ESCC cells, while the impaired glycolytic phenotype was prominently restored by miR-26a-5p inhibitor or KPNA2 overexpression plasmid (**Figure 5E**). Additionally, OCR detection revealed that silencing PCED1B-AS1 significantly elevated basal and maximal OCR values, indicating enhanced mitochondrial oxidative phosphorylation, and this metabolic shift was evidently reversed by inhibiting miR-26a-5p or overexpressing KPNA2, which brought the oxidative respiration level back close to the baseline (**Figure 5F**).

KPNA2 knockdown reverses the effects of PCED1B-AS1 overexpression on ESCC cell malignancy and glycolysis

As shown in **Figure 6A-D**, PCED1B-AS1 overexpression promoted ESCC cell proliferation while

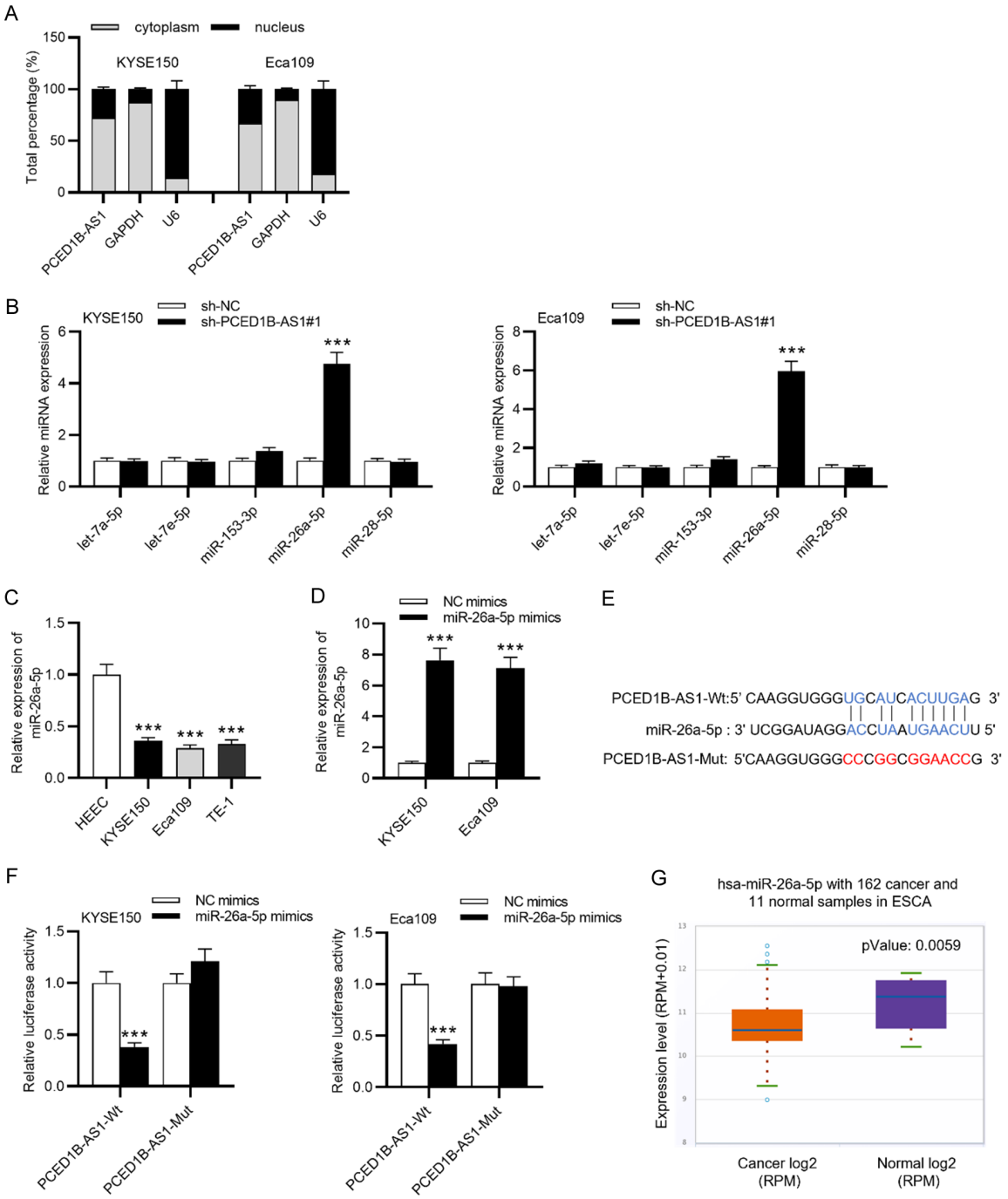
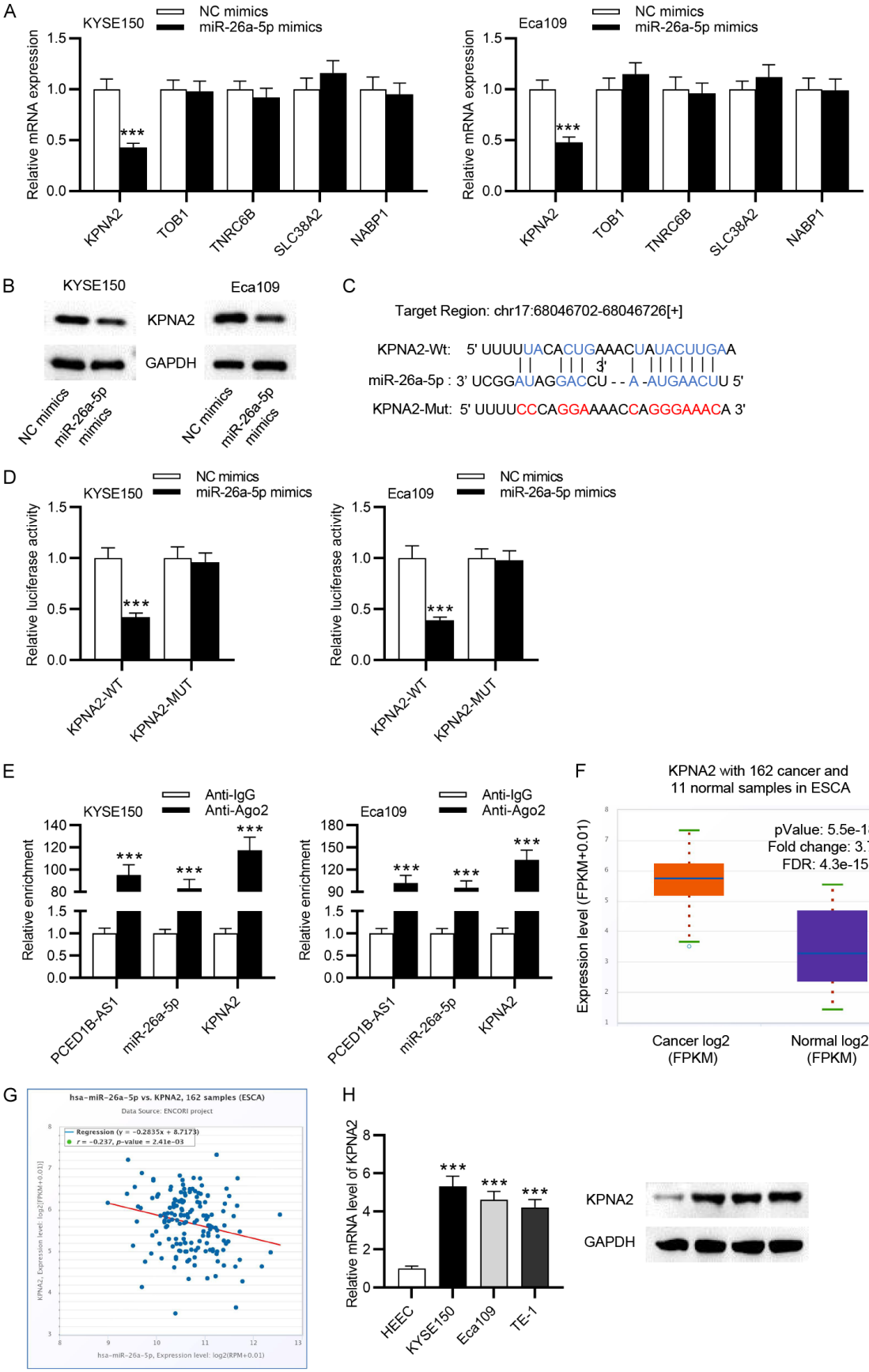


Figure 3. PCED1B-AS1 interacts with miR-26a-5p in ESCC cells. A. RNA fractionation assay was performed to determine the localization of PCED1B-AS1 in ESCC cells. B. LncRNA database (Lncbase) v3 was used to predict downstream miRNAs of PCED1B-AS1, and the expression levels of these miRNAs were detected in KYSE150 and Eca109 cells transfected with sh-NC or sh-PCED1B-AS1#1. C. RT-qPCR was used to evaluate miR-26a-5p expression in HEEC, Eca109, TE-1, and KYSE150 cells. D. RT-qPCR was used to detect miR-26a-5p expression in KYSE150 and Eca109 cells transfected with NC mimics and miR-26a-5p mimics. E. The binding site between PCED1B-AS1 and miR-26a-5p was predicted by bioinformatics analysis. F. Dual-luciferase reporter assays were conducted to verify the binding of miR-26a-5p to PCED1B-AS1 in ESCC cells transfected with NC mimics or miR-26a-5p mimics. G. Encyclopedia of RNA interactomes (ENCORI) was used to detect miR-26a-5p expression in ESCA tissues. n=3. ***P<0.001 versus sh-NC, HEEC, or NC mimics group.


A
KYSE150
NC mimics
miR-26a-5p mimics
Relative mRNA expression
KPNA2
TOB1
TNRC6B
SLC38A2
NABP1
Eca109
B
KYSE150
Eca109
KPNA2
GAPDH
NC mimics
miR-26a-5p mimics
C
Target Region: chr17:68046702-68046726[+]
KPNA2-Wt: 5' UUUUUACACUGAAACUAUACUUGAA
miR-26a-5p : 3' UCGGAUAGGACCU - - A -AUGAACUU 5'
KPNA2-Mut: 5' UUUUCCCAGGGAAACCAGGGAAACA 3'
D
Relative luciferase activity
KPNA2-WT
KPNA2-MUT
E
Anti-IgG
Anti-Ago2
Relative enrichment
PCED1B-AS1
miR-26a-5p
KPNA2
F
KPNA2 with 162 cancer and
11 normal samples in ESCA
pValue: 5.5e-18
Fold change: 3.71
FDR: 4.3e-15
Expression level (FPKM+0.01)
Cancer log2 (FPKM)
Normal log2 (FPKM)
G
hsa-miR-26a-5p vs. KPNA2, 162 samples (ESCA)
Data Source: ENCORI project
Regression (y = -0.2835x + 8.7173)
r = -0.237, p-value = 2.41e-03
KPNA2, Expression level: log2[FPKM+0.01]
hsa-miR-26a-5p, Expression level: log2(RPM+0.01)
H
Relative mRNA level of KPNA2
HEEC
KYSE150
Eca109
TE-1
KPNA2
GAPDH

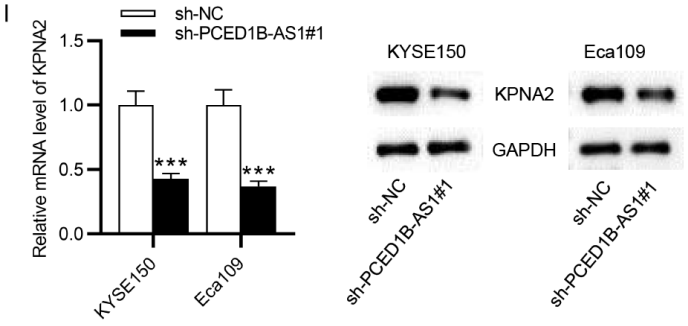


Figure 4. Karyopherin subunit alpha 2 (KPNA2) is a direct target gene of miR-26a-5p in ESCC cells. A. ENCORI was used to predict target genes of miR-26a-5p, and RT-qPCR was performed to measure these target genes in ESCC cells transfected with NC mimics or miR-26a-5p mimics. B. Western blot analysis was used to determine KPNA2 protein expression in ESCC cells transfected with NC mimics or miR-26a-5p mimics. C. The binding site between miR-26a-5p and KPNA2 was predicted by bioinformatics analysis. D. Dual luciferase reporter assays were conducted to verify the binding of miR-26a-5p to KPNA2 in ESCC cells transfected with NC mimics or miR-26a-5p mimics. E. RNA immunoprecipitation (RIP) assays were used to validate the relationship among PCED1B-AS1, miR-26a-5p and KPNA2. F. ENCORI was used to predict KPNA2 expression in ESCA tissues. G. The expression correlation between miR-26a-5p and KPNA2 in ESCA tissues was analyzed using the ENCORI database. H. RT-qPCR and Western blot analysis were used to detect the mRNA and protein levels of KPNA2 in HEEC and three ESCC cell lines. I. RT-qPCR and Western blot analysis were used to detect the mRNA and protein levels of KPNA2 in ESCC cells transfected with sh-NC or sh-PCED1B-AS1#1. n=3. $^{***}P<0.001$ versus NC mimics group, anti-IgG group, HEEC group, or sh-NC group.

inhibiting apoptosis compared with the control group. Knockdown of KPNA2 exerted an opposite effect on ESCC cell growth to PCED1B-AS1 overexpression. Notably, KPNA2 depletion reversed the oncogenic effects mediated by PCED1B-AS1 upregulation. The trend in the OE-PCED1B-AS1 + sh-KPNA2 group was comparable to that in the miR-26a-5p inhibitor + sh-KPNA2 group (**Figure 6A-D**). Moreover, KPNA2 deficiency inhibited glucose uptake, lactate production, and glycolysis, and reversed the effects of OE-PCED1B-AS1 on these indicators (**Figure 6E-G**). The glucose uptake, lactate production, and glycolytic capacity in the miR-26a-5p inhibitor + sh-KPNA2 group is similar to those in the OE-PCED1B-AS1 + sh-KPNA2 group (**Figure 6E-G**).

PCED1B-AS1 knockdown inhibits xenograft growth in ESCC

To explore the in vivo role of PCED1B-AS1 in ESCC, xenograft assays were performed. As shown in **Figure 7A**, **7B**, PCED1B-AS1 knockdown significantly reduced tumor size and weight. Furthermore, the lactic acid content was significantly decreased in the context of PCED1B-AS1 deficiency (**Figure 7C**). RT-qPCR showed that PCED1B-AS1 and KPNA2 levels were markedly reduced, while miR-26a-5p expression was notably increased in the sh-PCED1B-AS1#1 group (**Figure 7D**). Consistently, the mRNA level of KPNA2 was prominently reduced in the context of PCED1B-AS1 knockdown (**Figure 7E**).

Discussion

Our results demonstrate that PCED1B-AS1 is markedly upregulated in ESCC and functions to promote proliferation and glycolysis. This oncogenic activity is mediated by PCED1B-AS1 acting as a molecular sponge for miR-26a-5p, which alleviates miR-26a-5p-dependent suppression of KPNA2. Rescue experiments verify that the ceRNA network is indispensable for ESCC progression.

The ceRNA regulatory paradigm represents a well-characterized mechanism by which lncRNAs participate in tumorigenesis. In ESCC, several miR-26a-5p-associated ceRNA axes, including LINC00657/miR-26a-5p/CKS2 and LINC00240/miR-26a-5p, have been reported to facilitate tumor progression [29, 30]. Notably, KPNA2, the downstream effector identified in the present study, has previously been validated as a direct target of the SNHG8/miR-411 axis in ESCC [32]. Our findings extend this body of knowledge by identifying a novel ceRNA circuit: PCED1B-AS1/miR-26a-5p/KPNA2. The observation that KPNA2 can be modulated by at least two distinct lncRNAs (SNHG8 and PCED1B-AS1) via separate miRNAs indicates

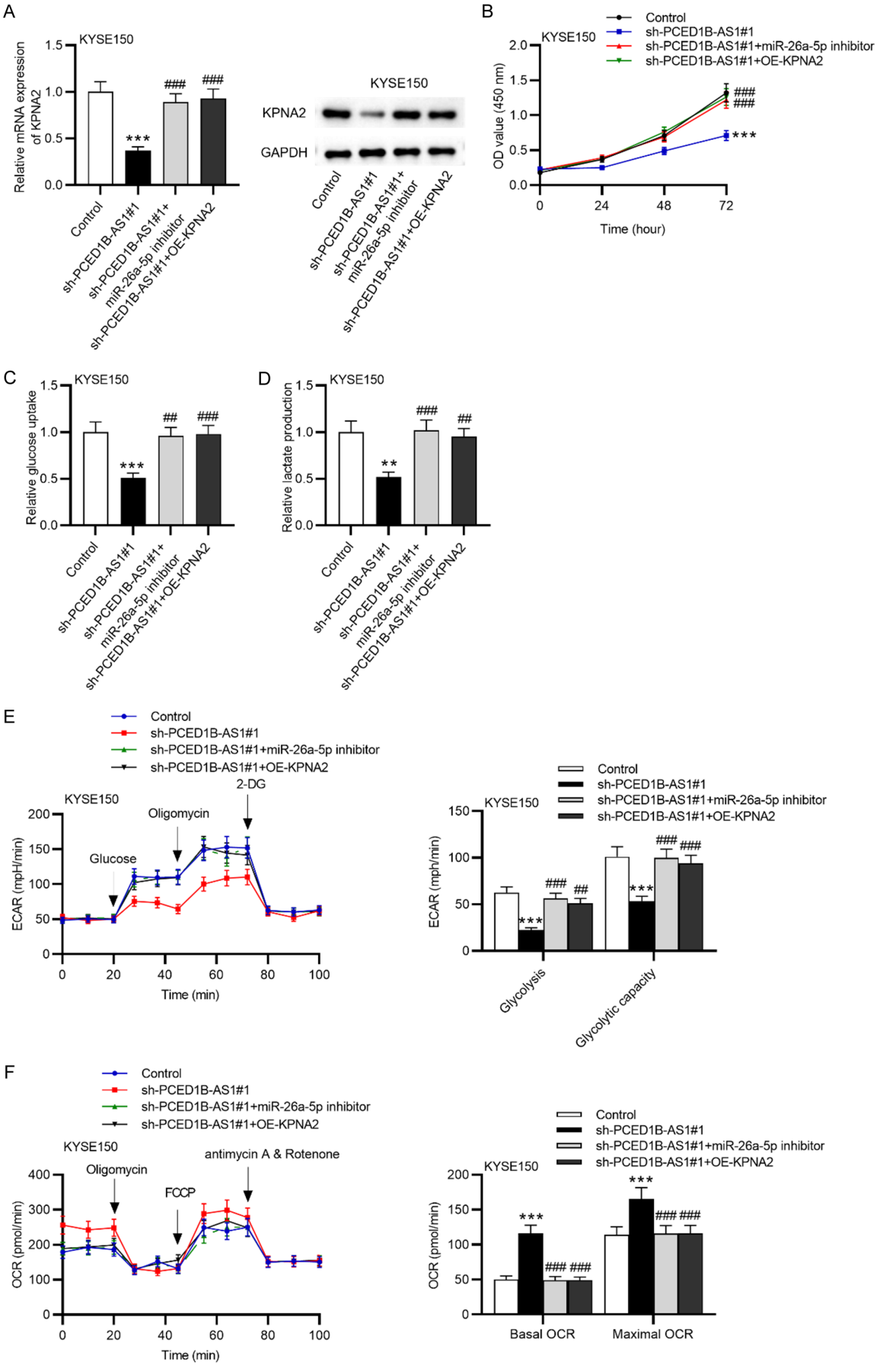

A
KYSE150
Relative mRNA expression of KPNA2
1.5
1.0
0.5
0.0
***
###
###
Control
sh-PCED1B-AS1#1
sh-PCED1B-AS1#1+ miR-26a-5p inhibitor
sh-PCED1B-AS1#1+OE-KPNA2
KYSE150
KPNA2
GAPDH
Control
sh-PCED1B-AS1#1
sh-PCED1B-AS1#1+ miR-26a-5p inhibitor
sh-PCED1B-AS1#1+OE-KPNA2
B
KYSE150
Control
sh-PCED1B-AS1#1
sh-PCED1B-AS1#1+miR-26a-5p inhibitor
sh-PCED1B-AS1#1+OE-KPNA2
OD value (450 nm)
2.0
1.5
1.0
0.5
0.0
0
24
48
72
Time (hour)
###
###
***
C
KYSE150
Relative glucose uptake
1.5
1.0
0.5
0.0
***
##
###
Control
sh-PCED1B-AS1#1
sh-PCED1B-AS1#1+ miR-26a-5p inhibitor
sh-PCED1B-AS1#1+OE-KPNA2
D
KYSE150
Relative lactate production
1.5
1.0
0.5
0.0
**
###
##
Control
sh-PCED1B-AS1#1
sh-PCED1B-AS1#1+ miR-26a-5p inhibitor
sh-PCED1B-AS1#1+OE-KPNA2
E
Control
sh-PCED1B-AS1#1
sh-PCED1B-AS1#1+miR-26a-5p inhibitor
sh-PCED1B-AS1#1+OE-KPNA2
KYSE150
Glucose
Oligomycin
2-DG
ECAR (mpH/min)
200
150
100
50
0
0
20
40
60
80
100
Time (min)
Control
sh-PCED1B-AS1#1
sh-PCED1B-AS1#1+miR-26a-5p inhibitor
sh-PCED1B-AS1#1+OE-KPNA2
KYSE150
ECAR (mph/min)
150
100
50
0
***
###
##
***
###
###
Glycolysis
Glycolytic capacity
F
Control
sh-PCED1B-AS1#1
sh-PCED1B-AS1#1+miR-26a-5p inhibitor
sh-PCED1B-AS1#1+OE-KPNA2
KYSE150
Oligomycin
FCCP
antimycin A & Rotenone
OCR (pmol/min)
400
300
200
100
0
0
20
40
60
80
100
Time (min)
Control
sh-PCED1B-AS1#1
sh-PCED1B-AS1#1+miR-26a-5p inhibitor
sh-PCED1B-AS1#1+OE-KPNA2
KYSE150
OCR (pmol/min)
200
150
100
50
0
***
###
###
***
###
###
Basal OCR
Maximal OCR

Figure 5. PCED1B-AS1 promotes ESCC cell proliferation and glycolysis by targeting miR-26a-5p and KPNA2. Cells in this figure were divided into four groups: control, sh-PCED1B-AS1#1, sh-PCED1B-AS1#1 + miR-26a-5p inhibitor, and sh-PCED1B-AS1#1 + OE-KPNA2. A. RT-qPCR and Western blot analysis were conducted to detect KPNA2 mRNA and protein levels in KYSE150 cells with the indicated transfection. B. CCK-8 assays were conducted to detect the viability of KYSE-150 cells. C, D. Commercial reagent kits were used to detect glucose uptake and lactate production in transfected KYSE-150 cells. E, F. ECAR and OCR in KYSE150 cells were determined using a Seahorse XFe96 extracellular flux analyzer. n=3. $^{**}P<0.01$, $^{***}P<0.001$ versus control group. $^{\#\#}P<0.01$, $^{\#\#\#}P<0.001$ versus sh-PCED1B-AS1#1 group.

that KPNA2 acts as a critical convergence node in ESCC pathogenesis. Such a regulatory architecture, in which multiple lncRNAs converge on a single effector transcript, may constitute a robust mechanism to maintain persistently high expression of this potent oncogene and sustain malignant cellular phenotypes.

Beyond defining this new regulatory axis, our study addresses a mechanistic question: how KPNA2, as the terminal effector, mediates the diverse oncogenic phenotypes induced by dysregulated PCED1B-AS1. KPNA2 is a key member of the karyopherin α family and governs nuclear import of cargo proteins bearing classical nuclear localization signals [33-35]. Its oncogenic function is attributed to the aberrant nuclear translocation of various transcription factors and signaling regulators. For example, in lung adenocarcinoma, KPNA2 enhances glycolysis by promoting nuclear accumulation of MYC, a master transcription factor controlling metabolic gene expression [31]. Building on this prior evidence, we propose a unified mechanistic model for ESCC: PCED1B-AS1/miR-26a-5p-mediated upregulation of KPNA2 may act as a central signaling amplifier that concurrently boosts nuclear import of multiple oncogenic cargoes such as MYC and signal transducer and activator of transcription 3 (STAT3). This coordinated event activates proliferative and anti-apoptotic transcriptional programs while rewiring cellular metabolism toward glycolysis, thereby explaining the concomitant increases in proliferation, attenuation of apoptosis, and glycolytic reprogramming observed in our model. Future work identifying the specific KPNA2-dependent cargo proteins in ESCC cells will be essential to validate this model and delineate the downstream transcriptional circuits.

Our findings carry meaningful clinical implications for ESCC management. The consistent upregulation of PCED1B-AS1 in ESCC tissues and cell lines, together with its central role in driving proliferation and glycolysis, renders this lncRNA a promising candidate diagnostic and prognostic biomarker. ESCC is frequently diagnosed at advanced stages owing to the absence of specific early symptoms, underscoring the urgent need for novel molecular markers to enable early detection. PCED1B-AS1 can be detected in tissue specimens and may also be measurable in liquid biopsies such as plasma or exosomes, raising the possibility of non-invasive screening and disease monitoring. Furthermore, the essential contribution of the PCED1B-AS1/miR-26a-5p/KPNA2 axis to ESCC pathogenesis identifies multiple actionable nodes for therapeutic intervention. Targeting oncogenic lncRNAs with antisense oligonucleotides or small interfering RNAs has emerged as a promising therapeutic strategy in preclinical cancer models. Alternatively, restoring miR-26a-5p activity using synthetic miRNA mimics may simultaneously suppress multiple oncogenic targets including KPNA2, providing a multi-pronged strategy to suppress tumor growth and metabolic reprogramming. Importantly, the convergence of diverse oncogenic signals onto KPNA2 suggests that direct inhibition of this nuclear transporter, using selective inhibitors currently under development, could disrupt a broad spectrum of downstream oncogenic pathways. Nevertheless, clinical translation of these findings will require rigorous validation in large multicenter cohorts to establish the sensitivity and specificity of PCED1B-AS1 as a biomarker, alongside comprehensive preclinical studies to evaluate the safety, efficacy, and delivery modalities of candidate therapeutics. Collectively, our study establishes a mechanistic foundation for developing PCED1B-AS1-oriented diagnostic and therapeutic strategies for this aggressive malignancy.

Several limitations of the presents study should be acknowledged. First, while our findings confirm the regulatory effect of PCED1B-AS1 on glycolytic reprogramming in ESCC, its potential involvement in other metabolic pathways,

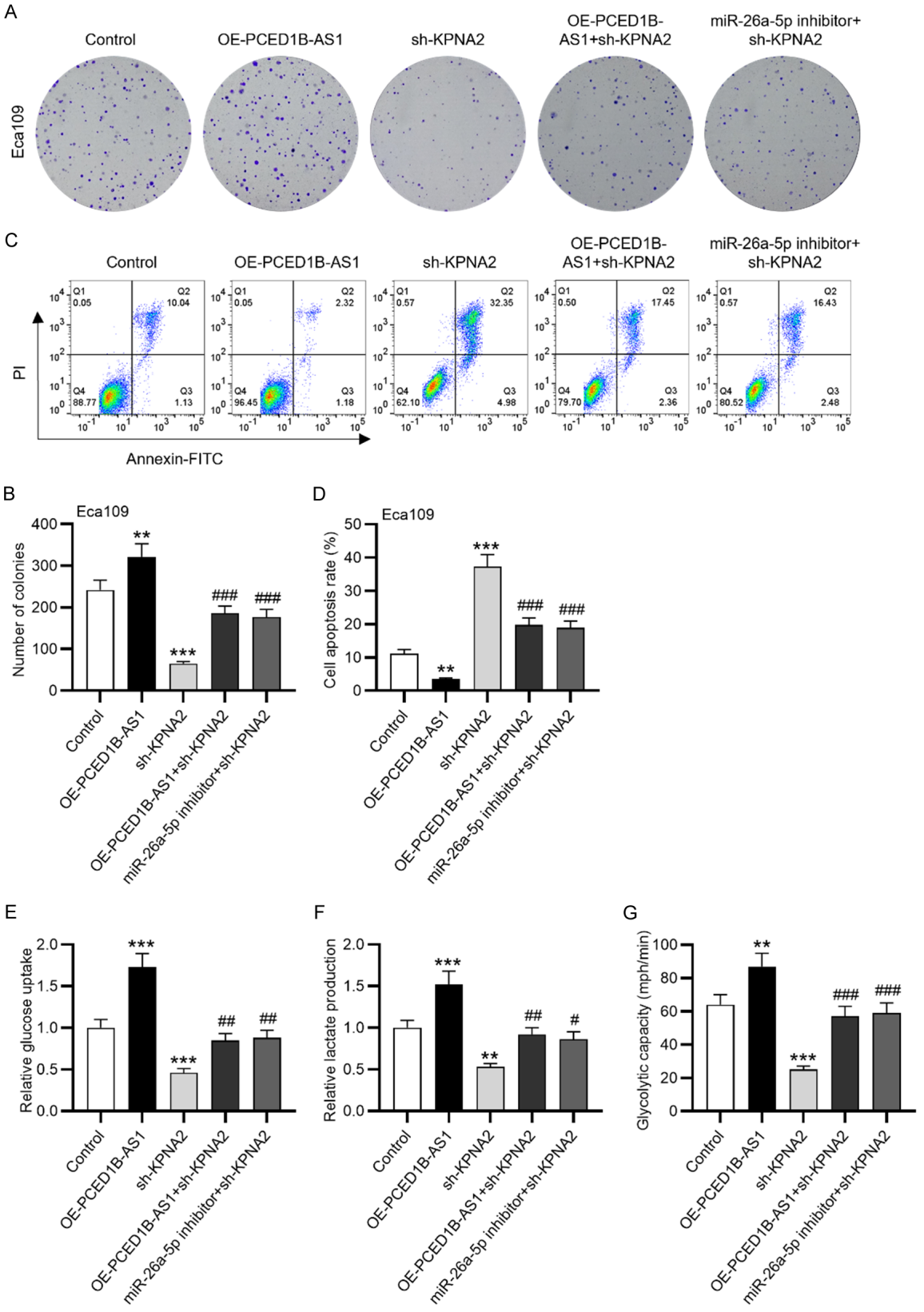


Figure 6. KPNA2 knockdown reverses effects of PCED1B-AS1 overexpression and miR-26a-5p inhibitor on ESCC cell malignancy and glycolysis. A, B. Colony formation assays was performed to measure ESCC cell proliferation. C, D. Flow cytometry analysis was conducted to assess ESCC cell apoptosis. E, F. Glucose uptake and lactate production

were measured using corresponding assay kits. G. ECAR after oligomycin treatment indicates glycolytic capacity. $^{**}P<0.01$, $^{***}P<0.001$ versus control group. $^{\#}P<0.05$, $^{\#\#}P<0.01$, $^{\#\#\#}P<0.001$ versus sh-KPNA2 group.

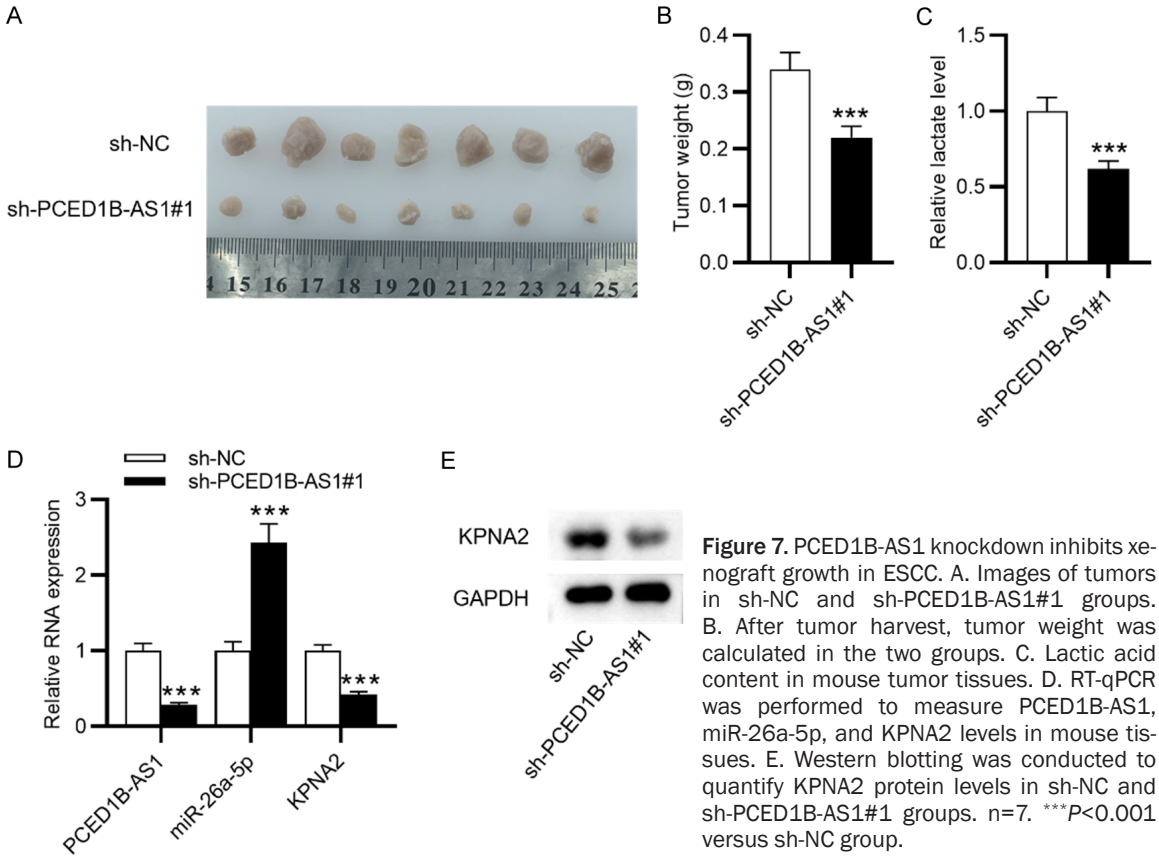


Figure 7. PCED1B-AS1 knockdown inhibits xenograft growth in ESCC. A. Images of tumors in sh-NC and sh-PCED1B-AS1#1 groups. B. After tumor harvest, tumor weight was calculated in the two groups. C. Lactic acid content in mouse tumor tissues. D. RT-qPCR was performed to measure PCED1B-AS1, miR-26a-5p, and KPNA2 levels in mouse tissues. E. Western blotting was conducted to quantify KPNA2 protein levels in sh-NC and sh-PCED1B-AS1#1 groups. n=7. $^{***}P<0.001$ versus sh-NC group.

including glutaminolysis and fatty acid oxidation, remains uncharacterized. Further investigations are therefore required to comprehensively clarify the metabolic regulatory spectrum of PCED1B-AS1. Second, no clinical samples were analyzed in the present study. Validation using large-scale, prospective clinical cohorts is necessary to confirm PCED1B-AS1 as a dependable diagnostic and prognostic biomarker for ESCC.

In conclusion, the current study identifies PCED1B-AS1 as a novel oncogenic lncRNA that promotes ESCC malignant progression and glycolytic metabolism via the miR-26a-5p/KPNA2 regulatory axis. By elucidating a previously unreported ceRNA mechanism underlying ESCC metabolic reprogramming, our study provides novel mechanistic insights into ESCC pathogenesis and highlight PCED1B-AS1 as a promising therapeutic target for the treatment of this aggressive gastrointestinal malignancy.

Acknowledgements

The authors appreciate all the participants providing support for this study. The manuscript was authored by the researchers. AI-assisted technologies were used solely for language polishing and editing. Specifically, Deepseek (version 4.1) and Doubao (version 2.31.1 win) were used for grammar, spelling, punctuation, readability improvement, and language editing. These tools were not used for study design, data collection, data analysis, interpretation of results, or generation of scientific content. The authors reviewed and revised all AI-assisted output and take full responsibility for the integrity, accuracy, and content of the manuscript. This work was supported by the Project of Huangshi Municipal Science and Technology Bureau (Grant number: KJ2025015).

Disclosure of conflict of interest

None.

Address correspondence to: Linyan Zhu, Hongbin Wang and Jing Lin, Department of Gastroenterology, Huangshi Central Hospital (Affiliated Hospital of Hubei Polytechnic University), No. 141 Tianjin Road, Huangshi 435000, Hubei, China. E-mail: 201931331034@stu.qhnu.edu.cn (LYZ); whbgolden@163.com (HBW); 13872059615@163.com (JL)

References

[1] Sato Y, Tanaka Y, Yokoi R, Tsuchiya H, Sengoku Y, Fukada M, Yasufuku I, Asai R, Tajima JY, Kiyama S, Kato T, Murase K and Matsuhashi N. Oligometastases of esophageal squamous cell carcinoma: a review. Cancers (Basel) 2024; 16: 704.

[2] Codipilly DC and Wang KK. Squamous cell carcinoma of the esophagus. Gastroenterol Clin North Am 2022; 51: 457-484.

[3] Waters JK and Reznik SI. Update on management of squamous cell esophageal cancer. Curr Oncol Rep 2022; 24: 375-385.

[4] Jiang W, Zhang B, Xu J, Xue L and Wang L. Current status and perspectives of esophageal cancer: a comprehensive review. Cancer Commun (Lond) 2025; 45: 281-331.

[5] Zhang X, Zheng X, Gao R, Wang Y, Wei T, Zang Z, Zhu L, Li Q, Zhang Y and Liu F. Role of diet in the risks of esophageal adenocarcinoma and squamous cell carcinoma: an updated umbrella review. Eur J Nutr 2024; 63: 1413-1424.

[6] Chiang HC, Hughes M and Chang WL. The role of microbiota in esophageal squamous cell carcinoma: a review of the literature. Thorac Cancer 2023; 14: 2821-2829.

[7] Simba H, Kuivaniemi H, Abnet CC, Tromp G and Sewram V. Environmental and life-style risk factors for esophageal squamous cell carcinoma in Africa: a systematic review and meta-analysis. BMC Public Health 2023; 23: 1782.

[8] Puhr HC, Prager GW and Ilhan-Mutlu A. How we treat esophageal squamous cell carcinoma. ESMO Open 2023; 8: 100789.

[9] An L, Li M and Jia Q. Mechanisms of radiotherapy resistance and radiosensitization strategies for esophageal squamous cell carcinoma. Mol Cancer 2023; 22: 140.

[10] Mitamura A, Tsujinaka S, Nakano T, Sawada K and Shibata C. Treatment strategies for locoregional recurrence in esophageal squamous-cell carcinoma: an updated review. Cancers (Basel) 2024; 16: 2539.

[11] Chen Y, Yu R and Liu Y. Combine radiotherapy and immunotherapy in esophageal squamous cell carcinoma. Crit Rev Oncol Hematol 2023; 190: 104115.

[12] Wei H, Fang R, Zhang S, Lin X and Li L. Current advances in the functional role of long non-coding RNAs in the oncogenesis and metastasis of esophageal squamous cell carcinoma: a narrative review. Transl Cancer Res 2025; 14: 2150-2167.

[13] Feng Q, Zhang H, Yao D, Chen WD and Wang YD. Emerging role of non-coding RNAs in esophageal squamous cell carcinoma. Int J Mol Sci 2019; 21: 258.

[14] Yan Q, Wong W, Gong L, Yang J, Liang D, Chin KY, Dai S and Wang J. Roles of long non-coding RNAs in esophageal cell squamous carcinoma (Review). Int J Mol Med 2024; 54: 72.

[15] Li H, Jia J, Yang L, Chu J, Sheng J, Wang C, Meng W, Jia Z, Yin H, Wan J and He F. LncRNA MIR205HG drives esophageal squamous cell carcinoma progression by regulating miR-214/SOX4 axis. Onco Targets Ther 2020; 13: 13097-13109.

[16] Liu Y, Li C, Fang L, Wang L, Liu H, Tian H, Zheng Y, Fan T and He J. Lipid metabolism-related lncRNA SLC25A21-AS1 promotes the progression of oesophageal squamous cell carcinoma by regulating the NPM1/c-Myc axis and SLC25A21 expression. Clin Transl Med 2022; 12: e944.

[17] Qiu BQ, Lin XH, Ye XD, Huang W, Pei X, Xiong D, Long X, Zhu SQ, Lu F, Lin K, Zhang XQ, Xu JJ, Sheng LL, Zhang XM, Zhang PF and Wu YB. Long non-coding RNA PSMA3-AS1 promotes malignant phenotypes of esophageal cancer by modulating the miR-101/EZH2 axis as a ceRNA. Aging (Albany NY) 2020; 12: 1843-1856.

[18] Feng Z, Li X, Qiu M, Luo R, Lin J and Liu B. LncRNA EGFR-AS1 upregulates ROCK1 by sponging miR-145 to promote esophageal squamous cell carcinoma cell invasion and migration. Cancer Biother Radiopharm 2020; 35: 66-71.

[19] Li Z, Qin X, Bian W, Li Y, Shan B, Yao Z and Li S. Exosomal lncRNA ZFAS1 regulates esophageal squamous cell carcinoma cell proliferation, invasion, migration and apoptosis via microRNA-124/STAT3 axis. J Exp Clin Cancer Res 2019; 38: 477.

[20] Li D, Li D, Meng L, Liu J, Huang C and Sun H. LncRNA NLIPMT inhibits tumorigenesis in esophageal squamous-cell carcinomas by regulating miR-320/Survivin axis. Cancer Manag Res 2020; 12: 12603-12612.

[21] Liu J, Liu ZX, Wu QN, Lu YX, Wong CW, Miao L, Wang Y, Wang Z, Jin Y, He MM, Ren C, Wang DS, Chen DL, Pu HY, Feng L, Li B, Xie D, Zeng MS, Huang P, Lin A, Lin D, Xu RH and Ju HQ. Long noncoding RNA AGPG regulates PFKFB3-mediated tumor glycolytic reprogramming. Nat Commun 2020; 11: 1507.

[22] Chelakkot C, Chelakkot VS, Shin Y and Song K. Modulating glycolysis to improve cancer therapy. Int J Mol Sci 2023; 24: 2606.

[23] Xie Y, Wang M, Xia M, Guo Y, Zu X and Zhong J. Ubiquitination regulation of aerobic glycolysis in cancer. Life Sci 2022; 292: 120322.
[24] Alberghina L. The warburg effect explained: integration of enhanced glycolysis with heterogeneous mitochondria to promote cancer cell proliferation. Int J Mol Sci 2023; 24: 15787.
[25] Yao Z, Zhang Q, Guo F, Guo S, Yang B, Liu B, Li P, Li J, Guan S and Liu X. Long noncoding RNA PCED1B-AS1 promotes the warburg effect and tumorigenesis by upregulating HIF-1α in glioblastoma. Cell Transplant 2020; 29: 963689720906777.
[26] Taheri M, Safarzadeh A, Hussen BM, Ghafouri-Fard S and Baniahmad A. LncRNA/miRNA/mRNA network introduces novel biomarkers in prostate cancer. Cells 2022; 11: 3776.
[27] Ghasemi T, Khalaj-Kondori M, Hosseinpour Feizi MA and Asadi P. lncRNA-miRNA-mRNA interaction network for colorectal cancer; An in silico analysis. Comput Biol Chem 2020; 89: 107370.
[28] Shetty A, Venkatesh T, Kabbekodu SP, Tsutsumi R and Suresh PS. LncRNA-miRNA-mRNA regulatory axes in endometrial cancer: a comprehensive overview. Arch Gynecol Obstet 2022; 306: 1431-1447.
[29] Zhang XM, Wang J, Liu ZL, Liu H, Cheng YF and Wang T. LINC00657/miR-26a-5p/CKS2 ceRNA network promotes the growth of esophageal cancer cells via the MDM2/p53/Bcl2/Bax pathway. Biosci Rep 2020; 40: BSR20200525.
[30] Liu Y, Li T, Peng C, Mao Q, Shen B, Shi M, Lu H, Xiao T, Yang A and Cheng C. Knockdown of long noncoding RNA LINC00240 inhibits esophageal cancer progression by regulating miR-26a-5p. Contrast Media Mol Imaging 2022; 2022: 1071627.
[31] Feng Q, Song Q, Han B, Deng Z, Yu R and Liang J. KPNA2 promotes lung adenocarcinoma progression by inducing glycolysis-assisted MYC nuclear translocation. Cytotechnology 2025; 77: 158.
[32] Song H, Song J, Lu L and Li S. SNHG8 is upregulated in esophageal squamous cell carcinoma and directly sponges microRNA-411 to increase oncogenicity by upregulating KPNA2. Onco Targets Ther 2019; 12: 6991-7004.
[33] Han Y and Wang X. The emerging roles of KPNA2 in cancer. Life Sci 2020; 241: 117140.
[34] Jia Y, Wang Q, Liang M and Huang K. KPNA2 promotes angiogenesis by regulating STAT3 phosphorylation. J Transl Med 2022; 20: 627.
[35] Yang X, Wang H, Zhang L, Yao S, Dai J, Wen G, An J, Jin H, Du Q, Hu Y, Zheng L, Chen X, Yi Z and Tuo B. Novel roles of karyopherin subunit alpha 2 in hepatocellular carcinoma. Biomed Pharmacother 2023; 163: 114792.

Table S1. Sequences of primers used for reverse transcription-quantitative PCR

Gene	Sequence
PCED1B-AS1	Forward: 5'-CTGGTGTGGTATGTTCACG-3'
	Reverse: 5'-AACACTCTGTCATTTCCCTG-3'
miR-26a-5p	Forward: 5'-ACACTCCAGCTGGGTTCAAGTAATCCAGGA-3'
	Reverse: 5'-TGGTGTCGTGGAGTCG-3'
KPNA2	Forward: 5'-GGAGAAATGTAAGCTCATTTCC-3'
	Reverse: 5'-ACCAATTTACAGTGCCCTG-3'
TOB1	Forward: 5'-TGCTACCTGAACAAGATCAC-3'
	Reverse: 5'-ACTTGGATTTCAAGCTGCA-3'
TNRC6B	Forward: 5'-GGAGGAAACAATGATTCATGG-3'
	Reverse: 5'-ATTATCTTCAGTCTGACTCAGC-3'
SLC38A2	Forward: 5'-CTGCTTTGTCACATAACGTG-3'
	Reverse: 5'-CAGCATAGACAGTCTGTGAG-3'
NABP1	Forward: 5'-GACCAGAGGGTATGCATCC-3'
	Reverse: 5'-GTATGGAATCTCGCATTGCG-3'
GAPDH	Forward: 5'-TCAAGATCATCAGCAATGCC-3'
	Reverse: 5'-CGATACCAAAGTTGTCATGGA-3'
U6	Forward: 5'-CTCGCTTCGGCAGCAGCACATATA-3'
	Reverse: 5'-AAATATGGAACGCTTCACGA-3'